Journal of Advanced Engineering Trends
ISSN : 2682 - 2091

Vol.43, No.2. July 2024

http://jaet.journals.ekb.eg

Numerical investigation on the hot spot stress at fatigue-prone details of UHPC reinforced orthotropic steel decks

Hesham Abdelbaset [(1)], Bin Cheng [(2)]

Department of Civil Engineering, Faculty of Engineering, Minia University[(1)]

Department of Civil Engineering, School of Naval Architecture, Ocean and Civil Engineering, Shanghai Jiao Tong University[(2)]

Abstract

Orthotropic steel decks (OSDs) have been widely used in long and medium-span steel bridges because of superior structural features such as lightweight, high load carrying capacity, and modular construction. However, OSD is reported as one of the most structures experiencing fatigue defects which could limit the service life of the bridge deck. Recently, Ultra-High-Performance Concrete (UHPC) has been employed as a top layer in OSDs to improve the whole stiffness of OSDs and enhance their fatigue resistance. In the current study, numerical investigation has been performed to explore the stress response at fatigue-prone details of OSDs under the effect of repeated vehicle loading. In addition, the effect of employing UHPC layer on the hot spot stress at sensitive fatigue locations has been investigated. Quadratic extrapolation approach has been adopted to estimate the hot spot stress at the weld toe of the considered welded details. Results indicated that the stresses at rib-to-floorbeam welded connection are the highest stresses among the considered fatigue-prone locations and thus more concerns should be paid for the enhancement of its fatigue resistance. The application of a 50 mm thick UHPC layer considerably minimized the hot spot stresses at critical locations of all the considered fatigue-prone details in OSDs which indicates the efficiency of employing UHPC layer in OSDs for improving their fatigue strength and providing an infinite fatigue life.

Keywords: Orthotropic steel decks, UHPC overlay, RD welded connection, RF welded connection, Hot spot stress.

1. Introduction

Orthotropic steel decks (OSDs) are widely used in different types of steel bridges including suspension bridges, cable-stayed bridges, and movable bridges [1,2]. This is because orthotropic steel decks possess several advantages including lightweight, high load carrying capacity, modular construction, and minimized traffic disturbance [3,4]. Furthermore, laboratory tests and in-service performance of OSDs if properly designed and built, OSDs could provide a 100-year service life with minimal maintenance [5,6]. Orthotropic steel decks (OSDs) are typically composed of a deck plate, which is longitudinally supported by closely spaced open or closed ribs and transversely by discrete floorbeams, as shown in Fig. 1 [7–9].

Revised:4 July , 2022, Accepted:7 September , 2022

Despite the superior features of orthotropic steel decks, one of the key issues with OSDs is their fatigue performance under cyclic loads [10–12]. Many fatigue cracks were detected at in-service OSDs for both highway and railway steel bridges in recent years as a result of repeated loads, which could limit the service life of such deck structures [13–15]. For example, fatigue cracks were detected in HuMeng Bridge and Jian Yin Bridge after being in-service for six and 13 years, respectively [16,17]. The observed fatigue cracks were initiated at several locations on the bridge deck including at rib-to-deck (RD) welded joint, at rib-to-floorbeam (RF) welded joint, deck plate splice, and rib splice [18].

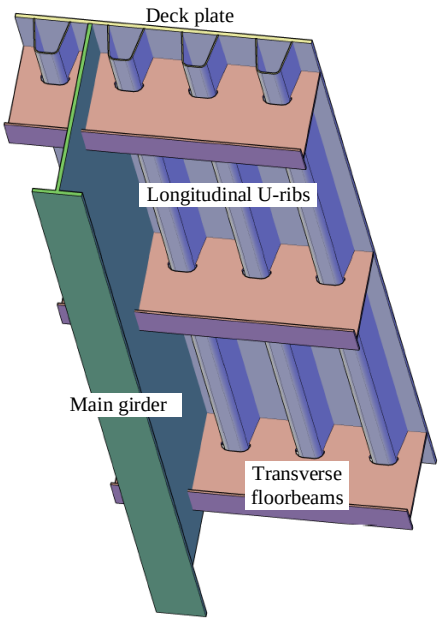

Fig. 1: Typical orthotropic steel deck

To avoid fatigue cracking prematurely, several studies have been performed to improve the fatigue strength of fatigue-prone details in OSDs, and a variety of fatigue strengthening approaches have been proposed [19–23]. Teixeira de Freitas et al. [24] used the bonded steel plate and sandwich steel plate systems for strengthening in-service OSDs, which rely on attaching a steel plate to the existing steel deck. Results demonstrated that using the bonded steel plate and the sandwich steel plate reduced the stresses at RD welded joint by 55% and by 45% respectively. Fiber-reinforced polymer (FRP) angles were employed by Liu et al. [25] to reinforce the cracked RD welded joints in OSDs. It was shown that adopting FRP angles considerably minimized the hot spot stress at vulnerable fatigue locations of RD welded joint and thus enhanced their fatigue lives. Large-size U-rib was used by Shao et al. [26] to minimize the welding amount and improve the fatigue resistance of fatigue-prone details in OSDs. It was noticed that employing the large-size U-rib minimized the amount of welding by about 38.7%, nevertheless, the stress reductions in case of normal U-rib and large-size one were similar [26]. A new rolled U-rib section with thickened edge was utilized by Heng et al. [27] instead of conventional U-rib so that the weld depth can be increased and thus improves the fatigue resistance of the RD welded joint. It was found that using thickened edge U-rib enhanced the fatigue life of RD welded joints from 4.19×10^6 to 8.59×10^6 load cycles reporting an increasing rate of 105% for the fatigue life.

Recently, Ultra-High-Performance Concrete (UHPC) has been employed instead of the traditional asphaltic layer to improve the whole stiffness of OSDs and enhance their fatigue resistance [28–32]. The new lightweight composite deck is shown in Fig. 2, which consists of the conventional OSD and a thin UHPC layer. In this study, a finite element analysis (FEA) is carried out to explore the stress response at sensitive fatigue regions (i.e., RD welded joint, RF welded joint, deck plate and rib splices) and compare their responses under the effect of wheel load. Furthermore, the effect of using UHPC overlay on the hot spot stress at sensitive fatigue locations of the studied details is clarified.

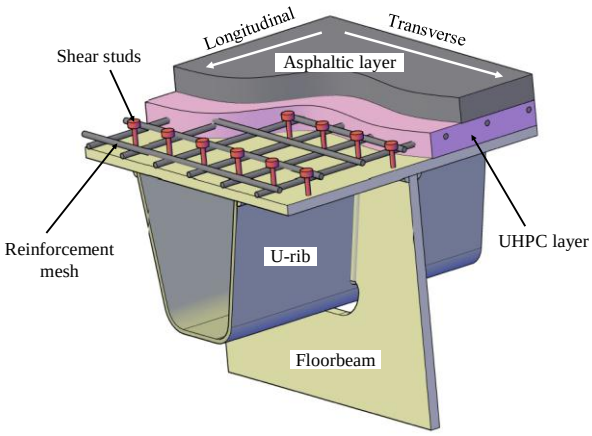

Fig. 2: Orthotropic steel deck reinforced by UHPC layer

2. Bridge information

The Sutong Bridge crosses the Yangtze River between Nantong and Changshu, is considered for the investigation in the current study. The Sutong Bridge is a super cable-stayed bridge with a main span of 1088 m and a bridge tower of 306 m in height, as shown in Fig. 3. Construction of the Sutong Bridge started in 2003 and opened for traffic in 2008. The bridge's completion reduces the time it takes to travel between Shanghai and Nantong from four hours to around one hour.

The bridge deck of the Sutong Bridge is a steel box girder, as indicated in Fig. 4. The bridge deck is an OSD with conventional longitudinal closed ribs (i.e., conventional U-ribs), which are supported by a series of transverse floorbeams. The U-rib was 300 mm in top width, 180 mm in bottom width, 300 mm in height, and 8 mm in thickness. The height of the U-rib varies between 290 mm to 300 mm. The floorbeam web thickness is 10 and 12 mm, whereas the 12 mm thick floorbeam was used for floorbeams anchored with stay cable. Deck plate thickness of 14 and 24 mm was used for the bridge construction, where the 24 mm thick deck plate was used at the region anchored to stay cables. Fig. 5 shows the detailed dimensions of the cross section used in this study. The spacing of

longitudinal ribs is 600 mm (i.e., center spacing), while the spacing of floorbeams is 4 m. The Sutong Bridge features a total of 272 cables, the longest of which is 577 m long. The stay cables were built of high-strength, low-relaxing 7 mm parallel steel wires. Q345qD and Q370qD steel were used to construct the bridge deck [26,33]. Standard segments with a length of 16 m were used to construct the box girder, while the segments nearing the end of the side span had a length of 12 m.

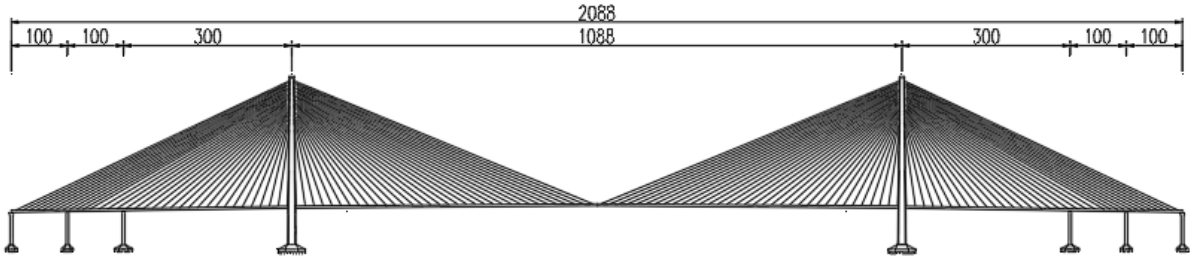

Fig. 3: Span layout of the Sutong Bridge (Units: m)

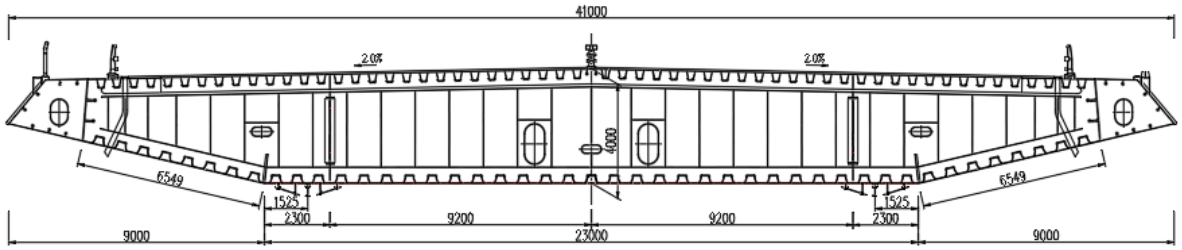

Fig. 4: Cross section of the Sutong Bridge (Units: mm)

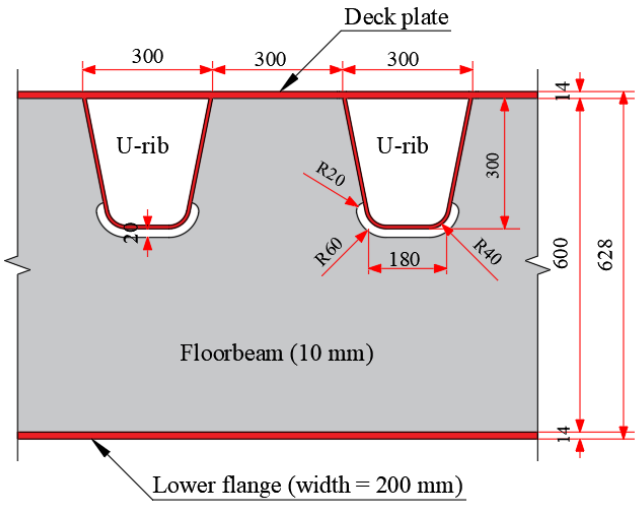

Fig. 5: Dimension of the OSD components (Units: mm)

3. Finite element analysis

3.1 FE model

To explore the stress response of vulnerable fatigue details under the effect of wheel loading in OSDs, a FE model of an OSD panel is established using ABAQUS software, as shown in Fig. 6. The fatigue-prone details considered herein are RD welded joint, RF welded joint, deck plate splice, and rib splice. Herein, the OSD panel model is 3.6 m wide and 12.0 m long, which consists of six longitudinal U-ribs and four transverse floorbeams. Two element types were used to establish the OSD panel with the area of interest simulated by the 8-node linear brick solid element (C3D8R) and the 4-node shell element (S4R) was used to simulate other parts of the OSD panel as shown in Fig. 6. The shell and solid segments of the OSD panel model were connected by Shell to Solid Coupling available in ABAQUS. The elastic modulus and the Poisson's ratio of steel material were set to be 210 GPa and 0.3, respectively.

The boundary conditions of the established OSD panel are as follows: (1) the vertical displacement

of all nodes at the bottom of the floorbeam was prevented to represent the vertical supports of the floorbeams; 2) nodes at the longitudinal ends were restricted from longitudinal translation (i.e., translation in *z*-direction) and rotation about the vertical direction (i.e., *y*- direction); and (3) nodes at side ends of the model were exerted with lateral constraints (i.e., translation in *x*-direction), to simulate the steel box girder transverse constraint on the model. According to the Saint-Venant principle since the fatigue-prone details of interest are far from the boundaries. Therefore, the boundary conditions should have limited influence on the analysis results [26,34].

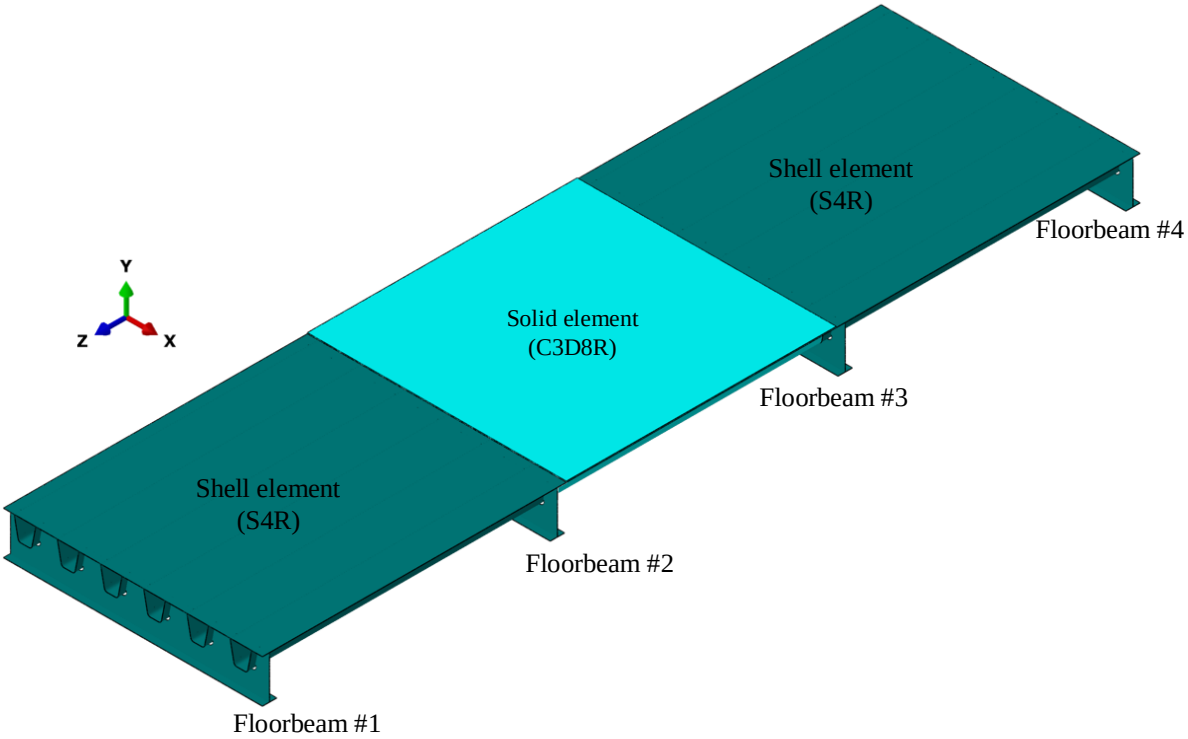

(a) FE model for RD welded detail and splices

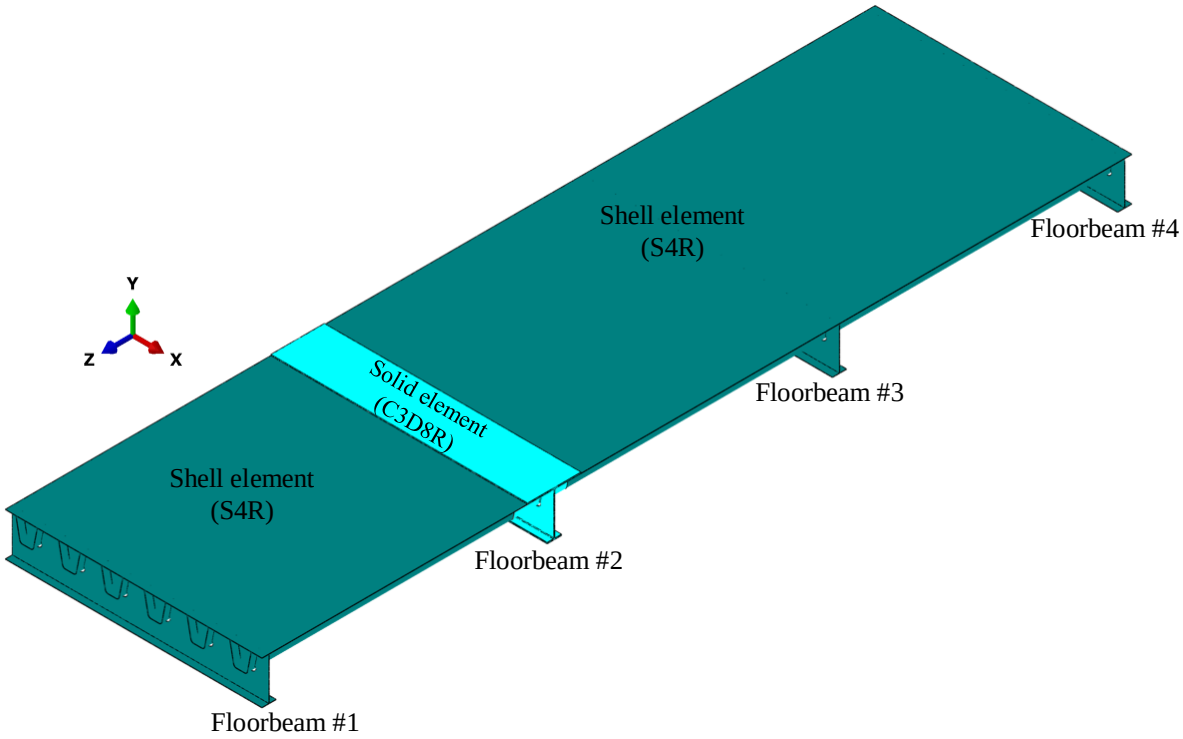

(b) FE model for RF welded detail

Fig. 6: FE model of the OSD panel

In the current investigation, the hot spot stress method is employed to determine the hot spot stresses at weld toes of the considered details. The hot spot stress is the appropriate approach for assessing the fatigue resistance of complex welded structural components (i.e., such as RD and RF welded joints in OSDs) that are most likely to have fatigue cracks at the weld toe. The hot spot stress can be obtained by several approaches such as the surface extrapolation approach (i.e., linear or quadratic extrapolation), through thickness linearization [35]. In the current study, the quadratic extrapolation method is adopted to determine the hot spot stress at weld toes of the sensitive fatigue details under consideration. As provided in the IIW recommendations [36], the hot spot stress can be obtained via quadratic extrapolation by using the following equation:

$$\sigma_{hs} = 2.52\,\sigma_{0.4\,t} - 2.24\,\sigma_{0.9\,t} + 0.72\,\sigma_{1.4\,t} \qquad (1)$$

Where, σ_{hs} is the hot spot stress at the weld toe, t is the plate thickness (i.e., deck plate thickness, rib web thickness, or floorbeam web thickness), $\sigma_{0.4t}$, $\sigma_{0.9t}$, and $\sigma_{1.4t}$ are the surface stress at reference points located at 0.4t, 0.9t, and 1.4t away from the weld toe.

According to IIW [35] specifications, the element mesh size near the hot spot area should be adequately refined, so that the hot spot stresses can be accurately determined. Therefore, fine mesh size was employed at fatigue-prone areas near weld toes (i.e., RD and RF weld toe) and around floorbeam cut-out edge, while coarser mesh was adopted in other parts as shown in Fig. 7 to keep the size of the model reasonable and save the computational time of the model.

3.2 Loading scheme

To explore the stress response at sensitive fatigue details considered in this study, the refined fatigue truck model provided in AASHTO LRFD specifications [37] was considered in this study. As shown in Fig. 8, the refined fatigue truck consists of two rear axles of 145 kN spaced at 9 m and one steering axle of 35 kN. Each rear axle consists of four wheels longitudinally spaced at 1.22 m and transversally at 1.8 m, and the wheel load patch area is 250 mm in the longitudinal direction and 510 mm in the transverse direction. While the steering axle consists of two wheels spaced at 1.22 m in the longitudinal direction and their load is distributed over an area of 250 × 250 mm.

According to the literature, it is concluded that the stress responses of fatigue-prone details in OSDs are particularly susceptible to local load effects of the applied wheel loads and a substantial response only could be observed when the wheel loads are positioned close to the detail under consideration [18,26]. Moreover, the distance between

floorbeams of the OSD panel of interest is 4 m which is considerably shorter than the distance between the rear axles. Consequently, only one rear axle group composed of four wheels of the refined fatigue truck is considered for the analysis herein, with the superimposition effect from the other truck axles ignored.

Three typical load cases are considered in the transverse direction which are LC1 over rib loading, LC2 riding rib web loading, and LC3 in between ribs loading, as depicted in Fig. 9. While in the longitudinal direction the load is moved forward every 1/16 *L*, where *L* is the spacing between floorbeams [26]. The center of the back wheel of the rear axle is chosen to determine the longitudinal position of wheel loads, which begins when it is centered on floorbeam #1 and ends when it reaches floorbeam #3.

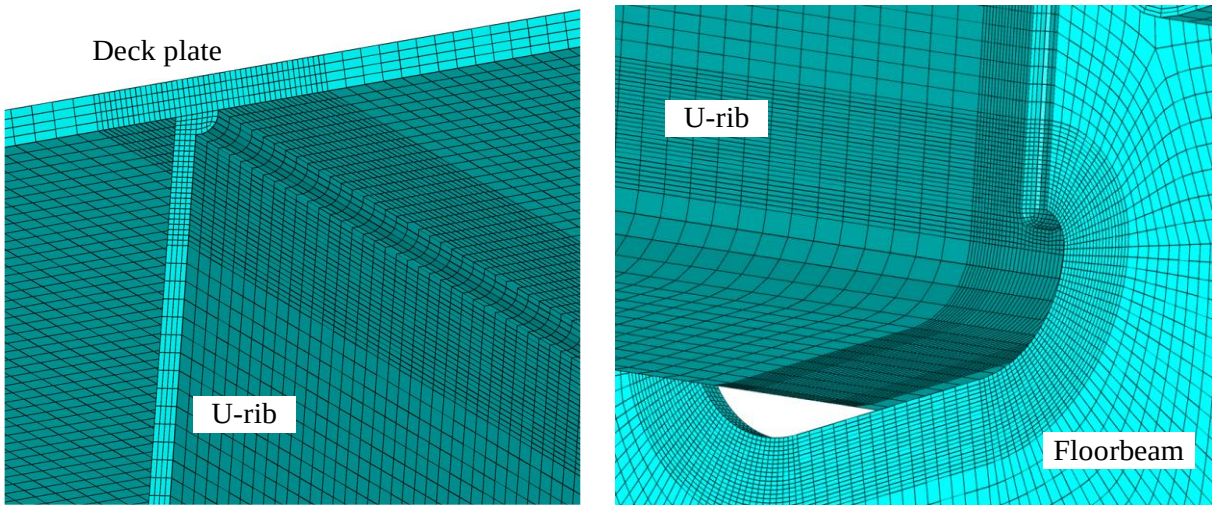

(a) Mesh details at rib-to-deck joint (b) Mesh details at rib-to-floorbeam joint

Fig. 7: Mesh density at the interest areas

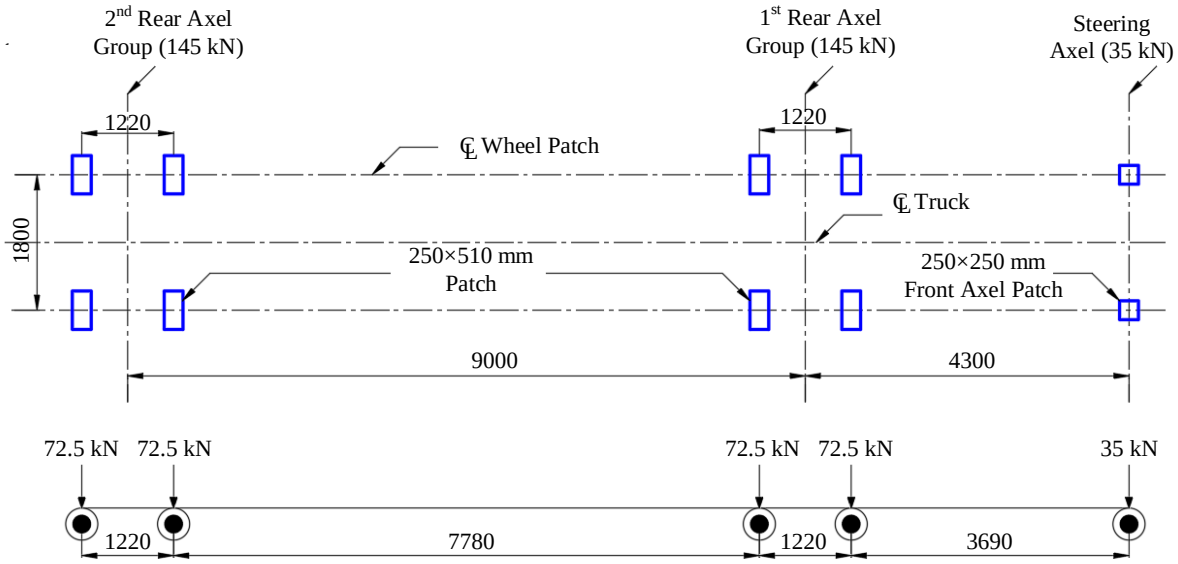

Fig. 8: Refined fatigue truck per AASHTO LRFD specifications [37]

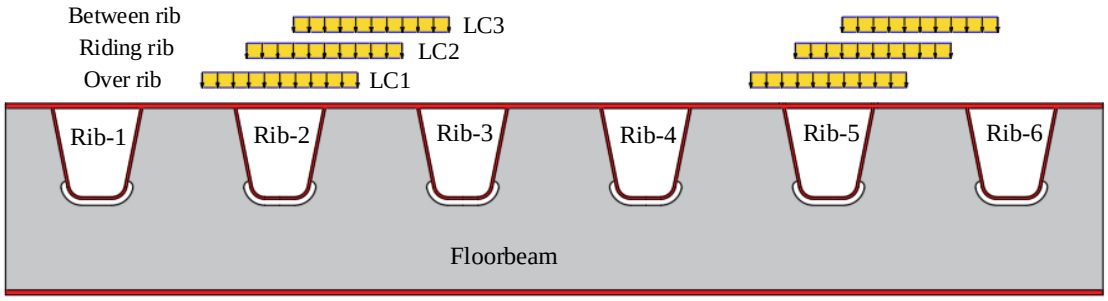

(a) Transverse load cases

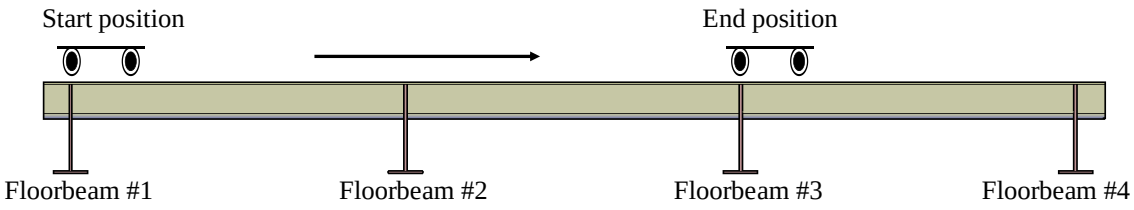

(b) Longitudinal load cases

Fig. 9: Load cases considered for the analysis

4. Results and discussion

4.1 RD welded joint

Fig. 10 presents the stress response of the RD welded joint on the left side of Rib 2, which is positioned in the mid span between floorbeam #2 and floorbeam #3, versus the longitudinal and transverse location of the wheel load. It is obvious from Fig. 10 that the transverse and longitudinal location of the wheel load considerably influenced the stress response at the deck and rib sides. The peak hot spot stress at the deck side is induced by LC1 with a stress magnitude of 13.2 MPa that is controlled by tension stress. While in the rib web side, the peak hot spot stress is 13.9 MPa under the effect of LC3 and controlled by tension stress as well. The stresses on the deck plate side are caused mainly due to the panel deformation from rib differential displacement and the local deformation of the deck plate in between the rib webs, as indicated in Fig. 11. While for case of the rib web side, the stresses are induced by the compression bending effect of the applied wheel loads and the deflection of the deck plate between the rib webs, as shown in Fig. 11.

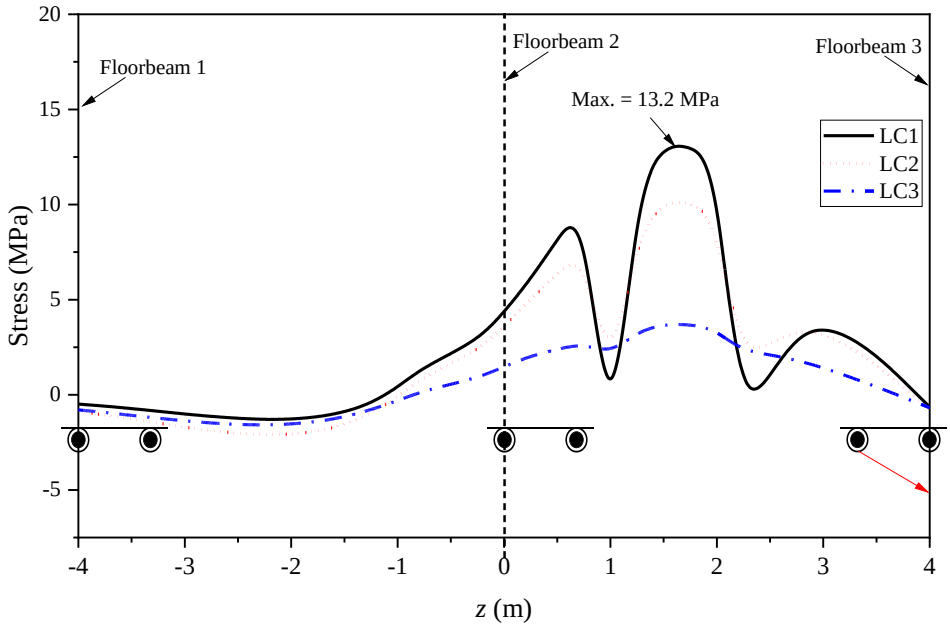

(a) Deck plate side

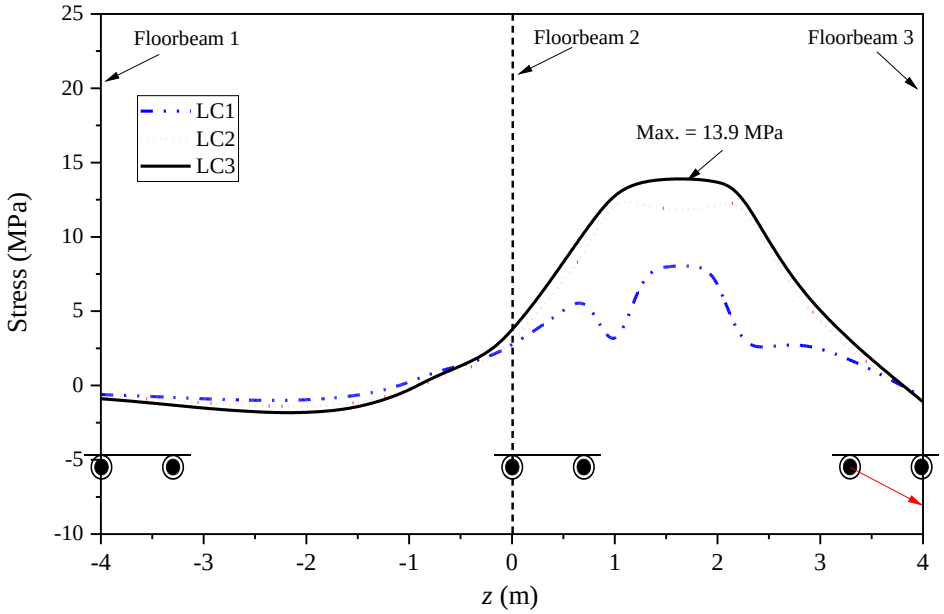

(b) Rib side

Fig. 10: Hot spot stress distribution at deck plate and rib sides of the RD welded joint

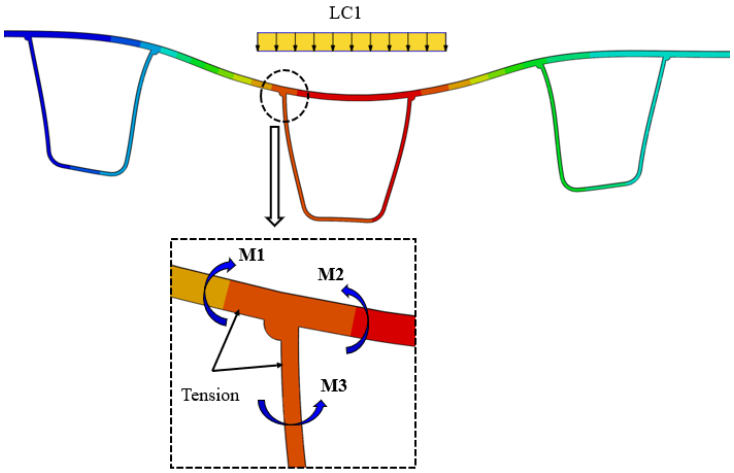

(a) LC1 deformed shape

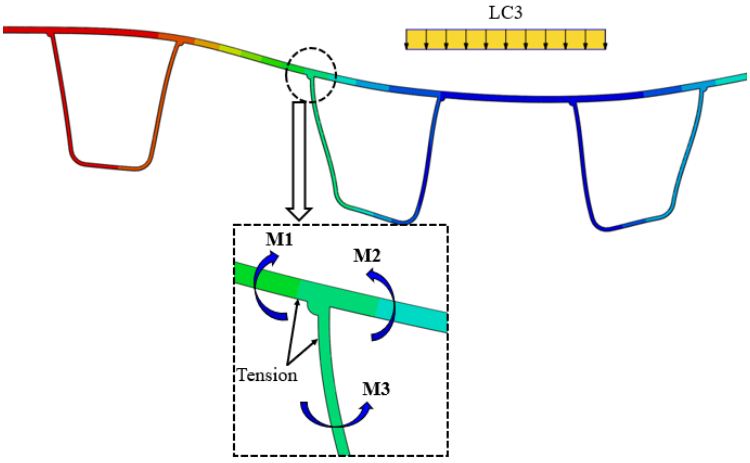

(b) LC3 deformed shape

Fig. 11: Deformation details due to LC1 and LC3 at RD joint

4.2 RF welded joint

In case of RF welded joint, the fatigue cracks could be initiated at RF weld toe or floorbeam cut-out edge. The stress at the critical locations of the RF welded joint is determined and presented herein, as shown in Fig. 12. Regarding σ_1 at RF weld toe, it is indicated that the hot spot stress is controlled by tension stresses due to the effect of the wheel loads, as depicted in Fig. 13 (a). The peak hot spot stress is induced by LC3 when the center of the back wheels is at a distance of 1 m from floorbeam #2 (i.e., z = 1.0 m), with the maximum hot spot stress of 73.6 MPa. Moreover, the peak hot spot stress on the floorbeam at RF weld toe (i.e., σ_2), is produced due to LC3 as well, when the tandem axle group is at 1.5 m from floorbeam #2 (i.e., z = 1.5 m), as depicted in Fig. 13 (b). Nevertheless, the hot spot stress magnitude of σ_2 is much lower than stress on the U-rib at RF weld toe (i.e., σ_1) which indicated that the fatigue cracks at σ_1 location are much more vulnerable to fatigue loading.

It is observed that the stress of the RF welded joint is primarily caused by large out-of-plane deformations of the U-rib because of no restraint at the bottom of the rib due to the presence of the floorbeam cut-out. Fig. 14 represents the displacement contour at RF welded joint under the effect of LC3. It is obvious from Fig. 14 that the out-of-plane deformation generated at the bottom of the U-rib is due to the rib web distortion and the presence of the floorbeam cut-out. In addition, the compression of the U-rib produced a secondary lateral expansion of the rib bottom which further resulted in an extra bending at the bottom of the U-rib. The stress distribution at the floorbeam cut-out edge is presented in Fig. 15. Two critical locations were reported as the sensitive locations at the floorbeam cut-out edge, as shown in Fig. 12.

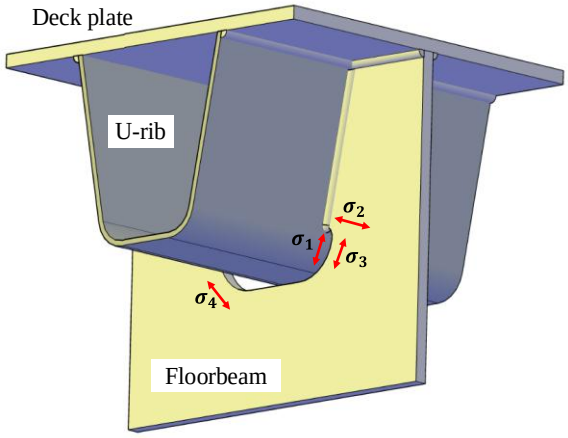

Fig. 12: Stresses and their directions at RF welded connection and at floorbeam cut-out edge

The three transverse load cases produced similar responses at both locations, however, the compression stress is obtained in one location and tension stress is prominent in the other location. Regarding σ_3, the maximum stress is observed due to LC3 when the wheel load at 0.25 m from floorbeam #2 (i.e., z = -0.25 m) with a considerably high compression stress of 145.7 MPa. While for case of σ_4, LC2 produced the maximum stress with a tension magnitude of 95.7 MPa. The highest stress level around the floorbeam cut-out edge was primarily caused by the out-of-plane distortion of the rib web and the in-plane distortion of the floorbeam web due to horizontal shear and vertical displacement of the floorbeam tooth [38].

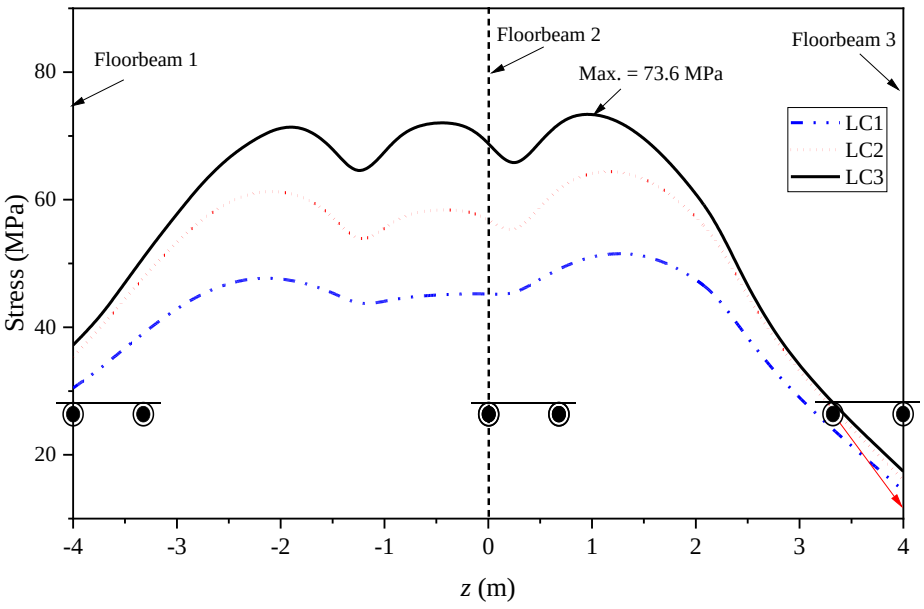

(a) σ_1

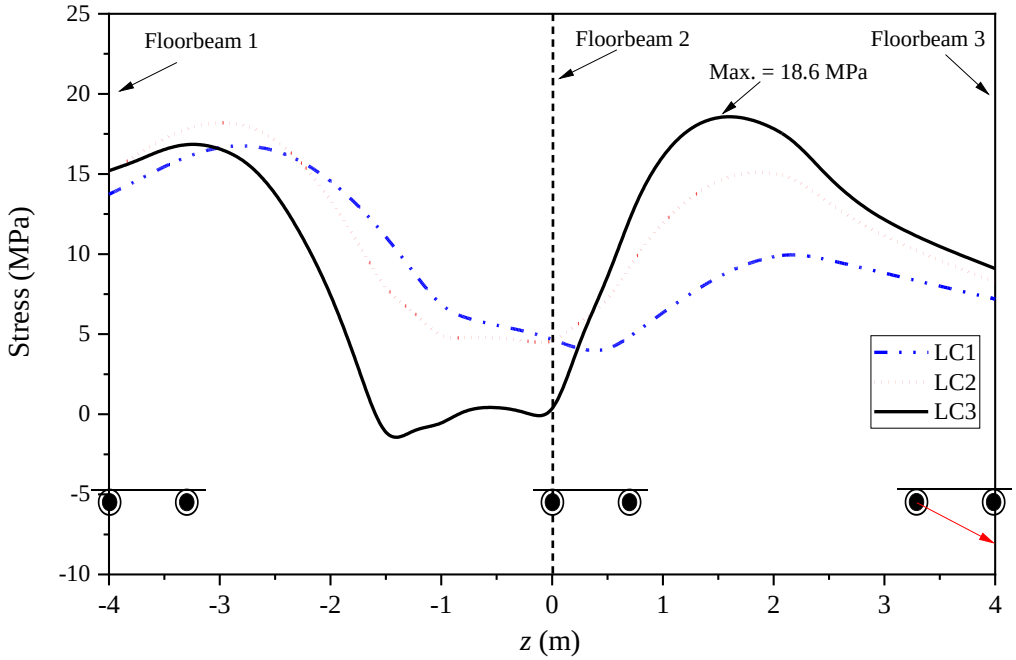

(b) σ_2

Fig. 13: Hot spot stress distribution at RF welded joint

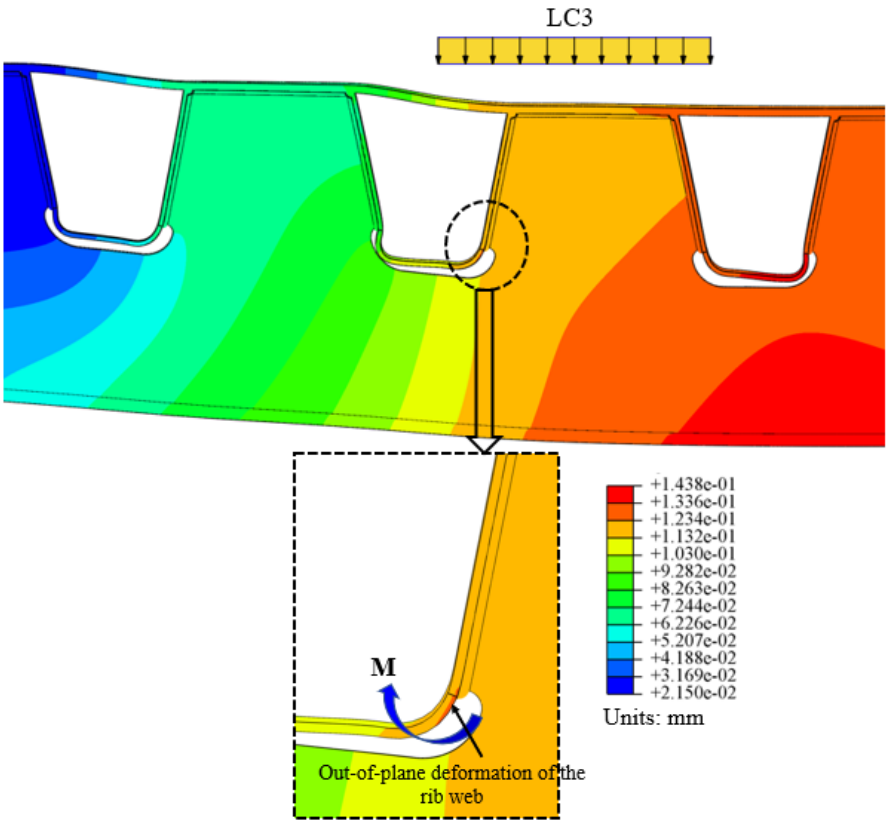

Fig. 14: Displacement contour due to LC3 at RF welded joint

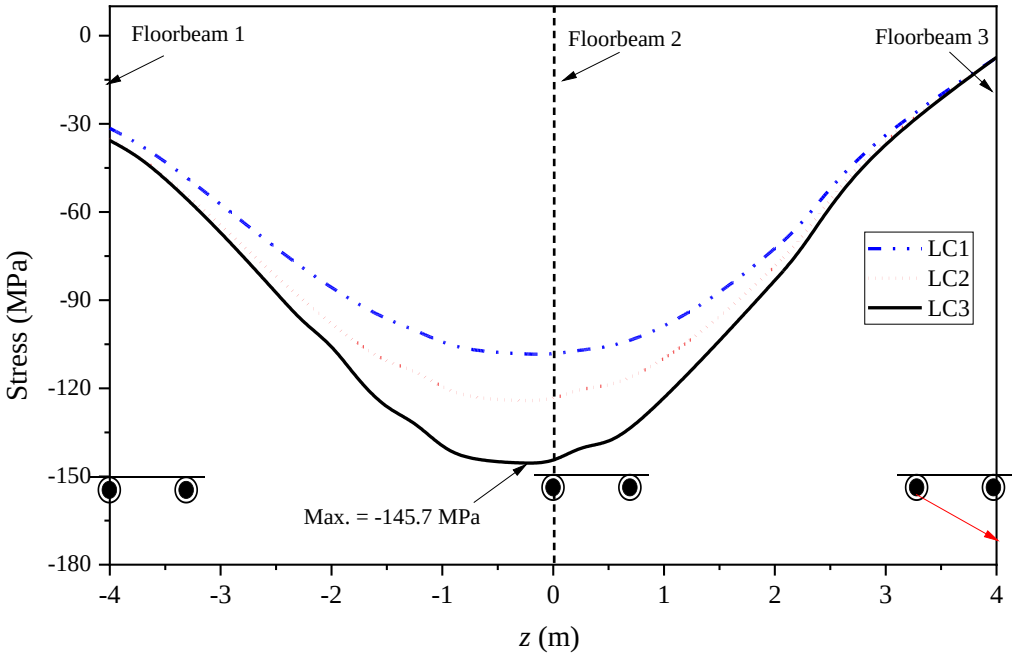

(a) σ_3

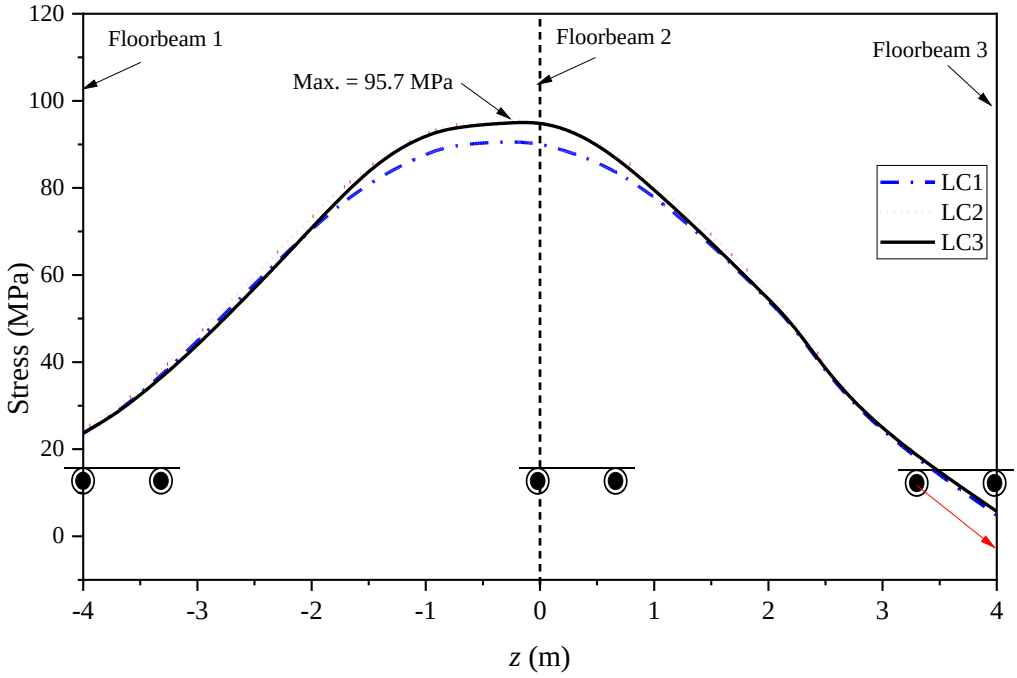

(b) σ_4

Fig. 15: Stress distribution at floorbeam cut-out edge

4.3 Deck plate splice

The deck plate splice is assumed at the quarter point of the rib span between floorbeam #2 and floorbeam #3 (i.e., z = 1 m). Fig. 16 shows the stress response at deck plate splice due to the effect of wheel loads versus the longitudinal location of the wheel load. It is observed that the stress changed from tension to compression with the moving of the applied wheel loads in the longitudinal direction. The obtained stress is remarkably low and its maximum stress equals 1.2 MPa produced due to LC3. Therefore, it is concluded that the deck plate splice is not so vulnerable to fatigue cracking such as other considered details (i.e., RD and RF welded joints).

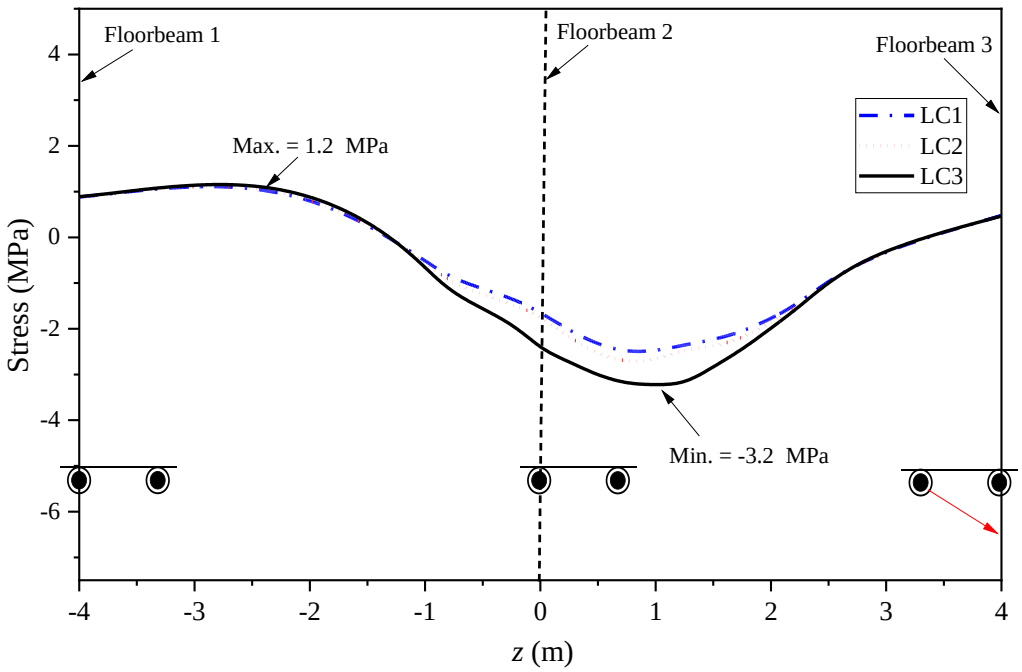

Fig. 16: Nominal stress at deck plate splice

4.4 Rib splice

The rib splice is considered at 0.8 m away from the floorbeam (i.e., z = 0.8 m) close to floorbeam #2. The stress at the middle of the bottom part of the rib is obtained and evaluated for the rib splice. Fig. 17 introduces the nominal stress response at the bottom part of the rib versus the longitudinal position of the wheel load due to the effect of the three considered transverse load cases. Results indicated that the maximum stress at the rib splice location was produced due to the effect of loading case LC1 when the wheel load is 1 m away from floorbeam 2 (i.e., z = 1 m). The obtained peak stress value is 16.7 MPa which is considerably higher than the stress of the deck plate splice, and consequently, it is concluded that the rib plate splice is more crucial for fatigue cracking than the deck plate splice.

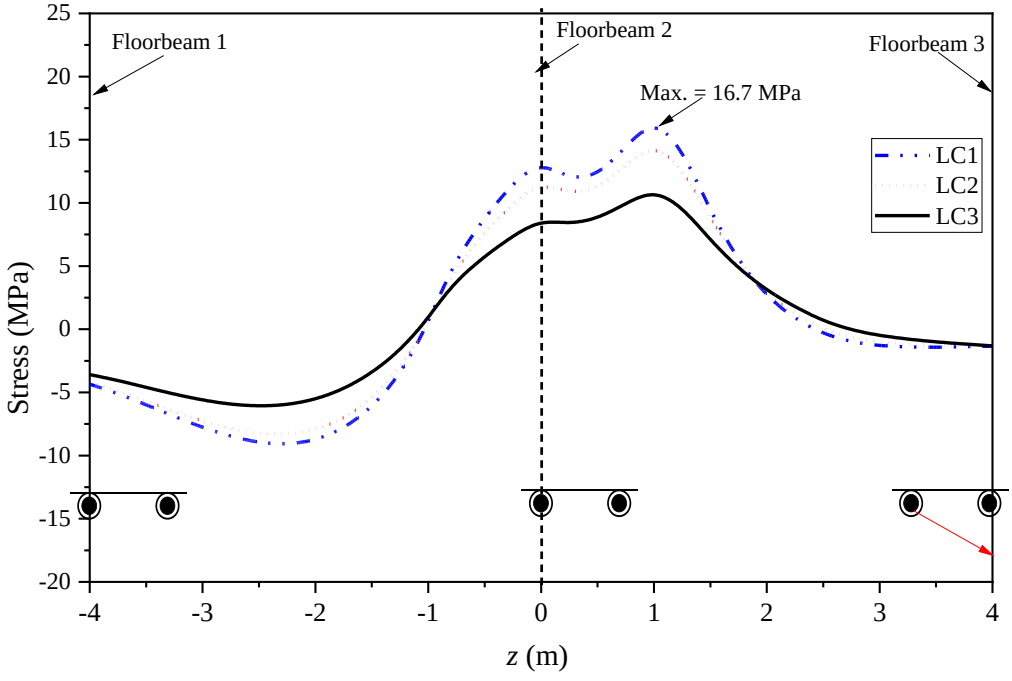

Fig. 17: Nominal stress at rib splice

4.5 Effect of UHPC layer

To study the effect of using UHPC layer on the hot spot stress of the studied details, a conventional OSD panel and OSD with UHPC overlay were analyzed. UHPC layer with a thickness of 50 mm was adopted herein, as shown in Fig. 18. Table 1 summarizes the stress ranges and reduction rates of the stress ranges at fatigue-prone details in OSD due to the use of UHPC layer. It is indicated that using a 50 mm thick UHPC layer, the stress at deck side of the RD joint was minimized by 65.9%, while a reduction rate of 52.5% was achieved at rib side. The reduction rate was 45.8% at rib surface of RF weld toe and the effect of UHPC layer on the detail is evident. While the stress on the floorbeam surface at RF weld toe was reduced by 47.3%. The minimal reduction rate is observed at the floorbeam cut-out edge, where the stress reductions were 25.3% and 34.9% at the floorbeam cut-out edges. For case of the deck and rib splices, the application of UHPC layer minimized the stress by 33.3% and 32.3%, respectively. In summary, the application of UHPC layer significantly reduced the hot spot stresses at fatigue-prone details in OSDs with the maximum reduction rate at RD joint and minimal reduction rate at floorbeam cut-out edge.

5. Conclusions

In this study the stress responses of the fatigue-prone details in OSDs were numerically investigated and the effect of using UHPC overlay was explored. The studied details include RD welded joint, RF welded joint, deck plate splice, and rib splice. Several load cases were studied in the longitudinal and transverse directions to capture the maximum stress of the details under consideration. According to the findings, the following remarks can be made:

(1) The determined stresses at RF welded joint are much higher than that at RD joint and thus the fatigue cracking of such detail is more critical under fatigue loading and more concerns should be paid for their fatigue resistance enhancement.

(2) Among the obtained stress at RF joint, the stress at RF welded toe (i.e., on the rib surface) and at floorbeam cut-out edge are the most critical stress, and fatigue cracks are expected to initiate first at RF weld toe or the edge of the floorbeam cut-out.

(3) The FEA results indicated that the stresses at deck plate splice are much lower than that of the other fatigue-prone details in the bridge deck. Therefore, the fatigue cracking of such splices is not so critical, and more attention should be paid to other fatigue-prone details (i.e., RD and RF welded details).

(4) The application of a 50 mm thick UHPC layer significantly minimized the stress at fatigue-prone details of OSDs. The stress reduction at RD locations varied between 52.5% to 65.9%, while for the RF joint the stresses reduced by 25.3% to 47.3%. Therefore, infinite fatigue life could be achieved for welded details of OSDs.

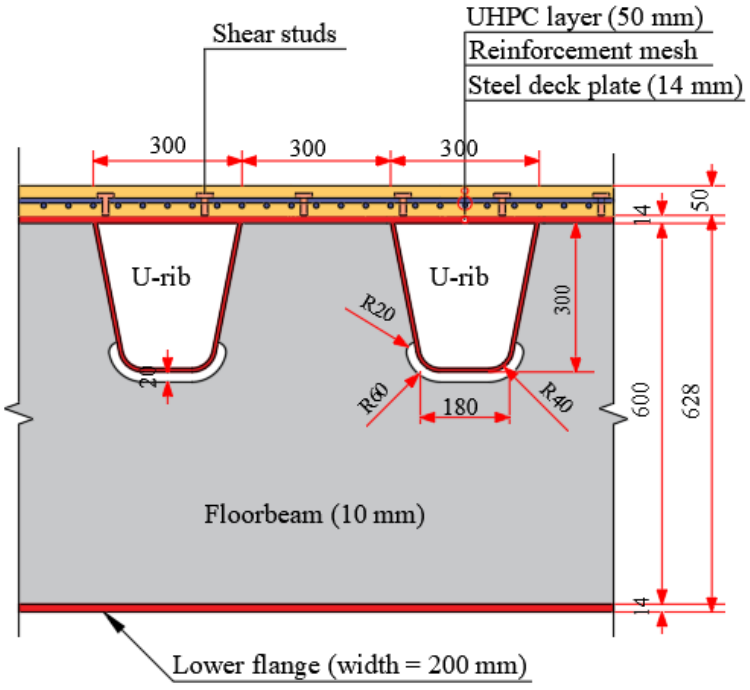

Fig. 18: Dimensions of OSD reinforced by UHPC layer

Table 1: Maximum stress ranges of fatigue-prone details

Fatigue location	Fatigue-prone detail	Maximum stress range (MPa)		Reduction rate of stress range (%)
		Without UHPC layer	With UHPC layer	
RD joint	Deck side	13.2	4.5	65.9
	Rib side	13.9	6.6	52.5
RF joint	σ_1	73.6	39.9	45.8
	σ_2	18.6	9.8	47.3
Floorbeam cut-out edge	σ_3	-145.7	-94.8	34.9
	σ_4	95.7	71.5	25.3
Deck plate splice		1.2	0.8	33.3
Rib splice		16.7	11.3	32.3

References

[1] M.H. Kolstein, Fatigue classification of welded joints in orthotropic steel bridge decks, Ph.D. thesis, Delft University of Technology, Delft, Netherlands; 2007.

[2] Z. Shi, S. Yang, Q. Pu, Y. Zhang, Fatigue Performance of Orthotropic Steel Decks in Long-Span Cable-Stayed Steel-Box Girder Railway Bridges, J. Bridg. Eng. 24 (2019) 1–13.

[3] P. Luo, Q. Zhang, Y. Bao, A. Zhou, Fatigue evaluation of rib-to-deck welded joint using averaged strain energy density method, Eng. Struct. 177 (2018) 682–694.

[4] Z. Zhu, Z. Xiang, J. Li, Y. Huang, S. Ruan, Fatigue behavior of orthotropic bridge decks with two types of cutout geometry based on field monitoring and FEM analysis, Eng. Struct. 209 (2020) 109926.

[5] K.J. Kitner, A Study of Manufacturable Rib-to-Floor Beam Connections in Steel Orthotropic Bridge Decks, Master thesis, Lehigh University, Bethlehem, 2016.

[6] S. Mukherjee, Laboratory Fatigue Evaluation of a Full Scale Steel Orthotropic Bridge Deck with Round Bottom Ribs and Fitted Floor Beams, Master thesis, Lehigh University, Bethlehem, USA; (2016).

[7] J. Maljaars, E. Bonet, R.J.M. Pijpers, Fatigue resistance of the deck plate in steel orthotropic deck structures, Eng. Fract. Mech. 201 (2018) 214–228.

[8] D. Li, J.H. Nie, W.X. Ren, W.H. Ng, G.H. Wang, Y. Wang, A novel acoustic emission source location method for crack monitoring of orthotropic steel plates, Eng. Struct. 253 (2022) 113717.

[9] B. Cheng, H. Abdelbaset, H.T. Li, L. Tian, J. Zhao, Fatigue behavior of rib-to-floorbeam welded connections in UHPC reinforced OSDs subjected to longitudinal flexural, Eng. Fail. Anal. 137 (2022) 106383.

[10] Y.S. Jeong, S. Kainuma, J.H. Ahn, Structural response of orthotropic bridge deck depending on the corroded deck surface, Constr. Build. Mater. 43 (2013) 87–97.

[11] Q. Wang, B. Ji, Z. Fu, Y. Yao, Effective Notch Stress Approach-Based Fatigue Evaluation of Rib-to-Deck Welds Including Pavement Surfacing Effects, Int. J. Steel Struct. 20 (2020) 272–286.

[12] J.W. Fisher, J.M. Barsom, Evaluation of Cracking in the Rib-to-Deck Welds of the Bronx–Whitestone Bridge, J. Bridg. Eng. 21 (2016) 04015065.

[13] S. Kainuma, M. Yang, Y.S. Jeong, S. Inokuchi, A. Kawabata, D. Uchida, Experimental investigation for structural parameter effects on fatigue behavior of rib-to-deck welded joints in orthotropic steel decks, Eng. Fail. Anal. 79 (2017) 520–537.

[14] M. Yang, S. Kainuma, Y.S. Jeong, Structural behavior of orthotropic steel decks with artificial cracks in longitudinal ribs, J. Constr. Steel Res. 141 (2018) 132–144.

[15] C. Cui, Y.L. Xu, Q.H. Zhang, Multiscale fatigue damage evolution in orthotropic steel deck of cable-stayed bridges, Eng. Struct. 237 (2021) 112144.

[16] Q. Wang, B. Ji, Z. Fu, Z. Ye, Evaluation of crack propagation and fatigue strength of rib-to-deck welds based on effective notch stress method, Constr. Build. Mater. 201 (2019) 51–61.

[17] B. Cao, Y. Ding, Z. Fang, F. Geng, Y. Song, Influence of weld parameters on the fatigue life of deck-ribwelding details in orthotropic

steel decks based on the improved stress integration approach, Appl. Sci. 9 (2019).

[18] Peter de Jong, Renovation techniques for fatigue cracked orthotropic steel bridge decks, Ph.D. thesis, Delft University of Technology, Delft, Nethrlands, 2006.

[19] P. Luo, Q. Zhang, Y. Bao, Y. Bu, Fatigue performance of welded joint between thickened-edge U-rib and deck in orthotropic steel deck, Eng. Struct. 181 (2019) 699–710.

[20] Y. Liu, X. Zhang, R. Liu, G. Chen, Design and Mechanical Properties of Steel-UHPC Lightweight Composite Decks, Adv. Civ. Eng. 2021 (2021).

[21] Z.Y. Chen, C.X. Li, J. He, H.H. Xin, Retrofit fatigue cracked diaphragm cutouts using improved geometry in orthotropic steel decks, Appl. Sci. 10 (2020).

[22] C.H. Ma, P. Deng, T. Matsumoto, Fatigue analysis of a UHPFRC-OSD composite structure considering crack bridging and interfacial bond stiffness degradations, Eng. Struct. 249 (2021) 113330.

[23] J. Di, J. Wang, X. Zhou, X. Peng, F. Qin, Fatigue Behavior of Rib-to-Floor Beam Junctions with Separate Inner Stiffeners in Orthotropic Steel Bridge Decks, J. Bridg. Eng. 27 (2022) 1–13.

[24] S. Teixeira De Freitas, H. Kolstein, F. Bijlaard, Fatigue Assessment of Full-Scale Retrofitted Orthotropic Bridge Decks, J. Bridg. Eng. 22 (2017) 1–16.

[25] J. Liu, T. Guo, D. Feng, Z. Liu, Fatigue Performance of Rib-to-Deck Joints Strengthened with FRP Angles, J. Bridg. Eng. 23 (2018) 1–14.

[26] X. Shao, W. Qu, J. Cao, Y. Yao, Static and fatigue properties of the steel-UHPC lightweight composite bridge deck with large U ribs, J. Constr. Steel Res. 148 (2018) 491–507.

[27] J. Heng, K. Zheng, C. Gou, Y. Zhang, Y. Bao, Fatigue Performance of Rib-to-Deck Joints in Orthotropic Steel Decks with Thickened Edge U-Ribs, J. Bridg. Eng. 22 (2017) 04017059.

[28] S. Zhang, X. Shao, J. Cao, J. Cui, J. Hu, L. Deng, Fatigue Performance of a Lightweight Composite Bridge Deck with Open Ribs, J. Bridg. Eng. 21 (2016) 04016039.

[29] Y. Huang, S. Chen, P. Gu, Numerical analysis on fatigue behavior of ultrahigh-performance concrete-Orthotropic steel composite bridge deck, Adv. Struct. Eng. 0 (2022) 1–16.

[30] H. Abdelbaset, B. Cheng, L. Tian, H. Li, J. Zhao, Enhancing fatigue resistance of rib-to-floorbeam welded connections in orthotropic steel bridge decks by using UHPC layer : An experimental study, Structures 36 (2022) 153–167.

[31] H. Abdelbaset, B. Cheng, L. Tian, H.T. Li, Q.H. Zhang, Reduce hot spot stresses in welded connections of orthotropic steel bridge decks by using UHPC layer: Experimental and numerical investigation, Eng. Struct. 220 (2020) 110988.

[32] B. Cheng, H. Abdelbaset, L. Tian, H.T. Li, Q. Su, Hot spot stress investigation on rib-to-deck-to-floor beam connections in UHPC reinforced OSDs, J. Constr. Steel Res. 179 (2021).

[33] JTG D64-2015, Specifications for Design of Highway Steel Bridge, Ministry of Transport of China, Beijing, China, China Communications Press, 2015 [In Chinese].

[34] Z. Zhu, T. Yuan, Z. Xiang, Y. Huang, Y.E. Zhou, X. Shao, Behavior and Fatigue Performance of Details in an Orthotropic Steel Bridge with UHPC-Deck Plate Composite System under In-Service Traffic Flows, 23 (2018) 1–21.

[35] E. Niemi, W. Fricke, S.J. Maddox, Fatigue Analysis of Welded Components: Designer's Guide to the Structural Hot-Spot Stress Approach, Paris, France; 2018.

[36] A.F. Hobbacher, Recommendations for fatigue design of welded joints and components. Rep No. IIW-2259-15/ex XIII-2460-13/XV-1440-13, Paris: International Institute of Welding, 2019.

[37] Sixth edition. AASHTO LRFD bridge design specifications. Washington, DC: American Association of State Highway and Transportation Officials; 2012.

[38] R. Connor, J. Fisher, W. Gatti, V. Gopalaratnam, B. Kozy, B. Leshko, et al. Manual for design, construction, and maintenance of orthotropic steel deck bridges. Report no. FHWA-IF-12-027. Washington, D.C., USA: Federal Highway Administration; 2012.